Accepted Manuscript

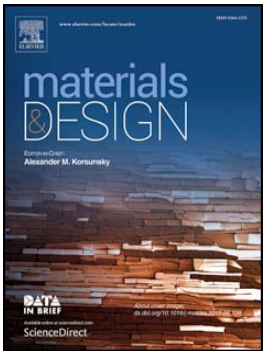

Preparation, corrosion, and wear resistance of Ni-Mo/Al composite coating reinforced with Al particles

R. Mousavi, M.E. Bahrololoom, F. Deflorian

PII: S0264-1275(16)31082-6
DOI: doi: 10.1016/j.matdes.2016.08.019
Reference: JMADE 2172

To appear in:

Received date: 29 April 2016
Revised date: 3 August 2016
Accepted date: 5 August 2016

Please cite this article as: R. Mousavi, M.E. Bahrololoom, F. Deflorian, Preparation, corrosion, and wear resistance of Ni-Mo/Al composite coating reinforced with Al particles, (2016), doi: 10.1016/j.matdes.2016.08.019

This is a PDF file of an unedited manuscript that has been accepted for publication. As a service to our customers we are providing this early version of the manuscript. The manuscript will undergo copyediting, typesetting, and review of the resulting proof before it is published in its final form. Please note that during the production process errors may be discovered which could affect the content, and all legal disclaimers that apply to the journal pertain.

ACCEPTED MANUSCRIPT

Preparation, corrosion, and wear resistance of Ni-Mo/Al composite coating reinforced with Al particles

R. Mousavi[a,1], M. E. Bahrololoom[a], F. Deflorian[b]

[a] Department of Materials Science and Engineering, Shiraz University, Shiraz, Iran.

[b] Department of Industrial Engineering, University of Trento, via Sommarive 9, Trento, Italy.

Abstract

In this research, Ni-Mo/Al composite coatings were deposited from a citrate bath containing Al metallic particles. The impact of Al particle content in the bath on the microstructure, texture, thickness, current efficiency, wear and corrosion behaviors of Ni–Mo/Al coatings was surveyed. The [200] preferred orientation developed slowly to the [111] orientation with increasing Al loadings in the bath. The results showed that electroplating at 40^{o}C and citrate ion concentration of 0.15M had the highest current efficiency and produced a dense coating free of cracks. Because of the presence of Mo, the morphology of the matrix changed from a regular pyramidal structure for Ni-Al composite coatings to cauliflower for Ni-Mo/Al composite coatings. The wear resistance of coatings decreased due to the increase of Al content in the coating. The polarization tests indicated that the corrosion resistance of the Ni-Mo/Al composite coating was enhanced by adding Al metal particles. This was due to the increase of Al content and decrease of the grain size of the coatings.

Key words: Ni-Mo/Al, composite coating, current efficiency, microhardness, wear, corrosion.

[1] Corresponding author: Mousavi@scu.ac.ir

ACCEPTED MANUSCRIPT

1. Introduction

Electrodeposotion of the nickel and its alloys have excellent wear and corrosion resistance [1-3].

Electrodeposition is an easy, cheap, and low temperature process for preparation of coatings [4, 5]. Composite electrodeposition may be done from a plating solution in which micron- or submicron-sized particles are suspended; Faradaic and electrophoretic mechanisms move variable amounts of these particles to the cathode and then they are embedded in the composite electrodeposit [6].

Many researchers have reported that adding fine solid particles to the nickel electrodeposit enhances the mechanical properties of coatings and many reviews of this technology are available [6-10]. Examples of included particles are (Al_2O_3 [11, 12], CeO_2 [13], SiC [14]), tribological characteristics (Al_2O_3 [11, 12], SiC [14, 15], Si_3N_4 [16]). Corrosion resistance (Al_2O_3 [11, 17, 18], CeO_2 [13, 19], SiC [18], Al [20]) and oxidation resistance (Al [20-25]) have been studied. In addition to increase corrosion and oxidation resistances by adding Al metal powder to the nickel matrix, as mentioned above, aluminum can also increase the adhesion between the coating and substrate [21].

According to the results reported by Susan *et al.* [26], the presence of Al metallic particles leads to grain refining. They showed that contrary to non-metallic particles, Al metallic particles can act as nuclei and hinder the grain growth.

Like other operating parameters such as pH, current density, and stirring rate, the amount of particles in the bath affects the amount of embedded particles in the coatings. Bostani *et al*. and Ramesh Bapu *et al.* have reported that there is a critical amount of particle after which the amount of deposited particles decreases by increasing the amount of particles in the solution [27,

ACCEPTED MANUSCRIPT

28]. This characteristic has been observed in different electrodeposited composite coatings and reported by several researchers [21, 29-33]. Therefore, the particle loading in the bath can induce different microstructures and properties of the coatings.

Most of the mentioned references have used pure nickel as the matrix. To the authors' knowledge, Ni-Co/Al and Ni-Cu/Al composite coatings were reported by references [20, 34, 35] in which Al metal powder was deposited in the Ni-based alloy matrix. The advantage of choosing Ni-Mo matrix is that alloys containing molybdenum have higher hardness, thermal and corrosion resistance [3, 36]. A mixture of Ni, Mo and Al powders is also known as self-bonding composite powders which are usually sprayed by plasma or by flame [37]. It is claimed that these types of coatings have high bonding strength and excellent resistance to wear and thermal shock [38, 39], and creep [40]. It has been shown that adding Al element to the Ni-Mo alloys increases sulfidation resistance at high temperatures. The sulfidation rate of this alloy has been attributed to the combined presence of both Al_2S and $Al_{0.55}Mo_2S_4$ [41, 42].

This study has been undertaken to obtain Ni–Mo coatings, containing Al particle as additional metallic component from acidic pH using a citrate solution bath. After finding a proper bath temperature and composition with high current efficiency, Ni–Mo/Al composite coatings were electrodeposited from an electrolyte containing different loadings of Al particles. Then, the effect of Al loading in the bath on the microstructure and properties of Ni-Mo/Al composite coatings was investigated.

ACCEPTED MANUSCRIPT

2. Materials and methods

2.1 Composition of electrolytes and plating parameters

All chemical materials mentioned in Table 1 were obtained from Sigma-Aldrich unless otherwise noted. Different solutions were prepared from analytical grade purity chemicals dissolved in distilled water. The pH of solutions was adjusted at 4 by adding NaOH and H_2SO_4. Electrodeposition was carried out galvanostatically at a constant current density (30 mA/cm^2) for all trials. Planning of the experiments can be seen in Table 2. The electrodeposition was carried out for 2 hours.

Table 1 Chemical and operating parameters and their values

Parameter	Levels
Trisodium Citrate (M)	0.15, 0.3
Temperature (^{o}C)	25, 40, 50, 60
Nickel Sulphate (M)	0.5
Sodium Molybdate (M)	0.01
Al Content (g/l)	1, 5, 10, 25
CTAB (g/l)	0.3
SDS (g/l)	0.5
Stirring Rate (rpm)	500
pH	4

Table 2 Design of experiments for determining proper bath temperature and composition

Trials	Citrate ion concentration (M)	Temperature (^{o}C)
1	0.15	25
2	0.15	40
3	0.15	50
4	0.3	25
5	0.3	40
6	0.3	50

The morphology of Al powder is shown in Figure 1. It is seen that the average size of Al powders is about 1μm.

ACCEPTED MANUSCRIPT

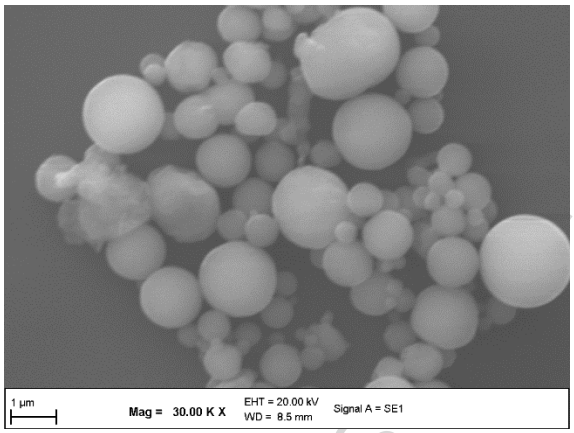

Figure 1 SEM image of Al powder used in this study.

2.2 Preparation of Substrate

Q-panels of carbon steel (SAE 1008/1010; 0.13 max C, 0.25–0.60 Mn) with dimentions of 4 cm* 1.5 cm were used as substrates or working electrodes. Before each deposition, the working electrode was polished with emery paper up to 1200 grade. After mechanical polishing, the substrate was electropolished in 95 vol.% acetic acid + 5 vol.% perchloric acid for 3 minutes. Finally, the substrate surface was activated in dilute sulfuric acid for 20s just before electrodeposition. Between each step, the specimens were washed in distilled water. The other sides and all side walls of the substrates were covered by a nonconducting epoxy resin, leaving only one surface of the plate exposed.

2.3 Electrodeposition of Ni–Mo/Al composite coatings

Electrodeposition was carried out in a 250 ml glass beaker with parallel electrodes positioned horizontally inside the electrolyte (the cathode was positioned under the anode).

ACCEPTED MANUSCRIPT

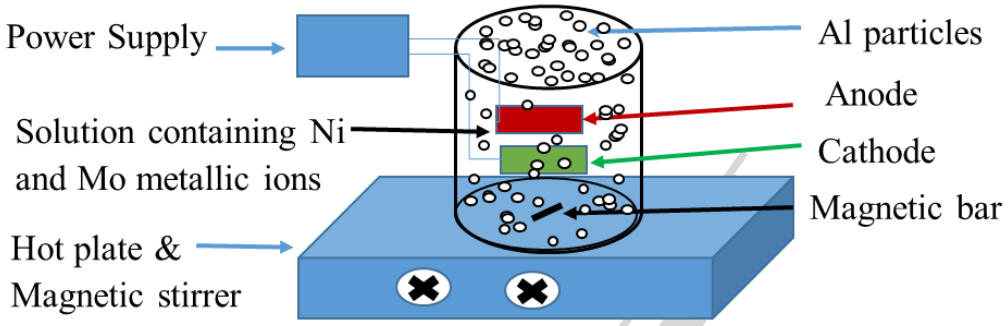

Figure 2 Schematic image of the electrodeposition setup.

Before each trial, the particles were initially blended with a little volume of the electrolyte and the required volume of the surfactant making it like a paste. Then the volume of the electrolyte was increased up to the required level, stirred well with a magnetic stirrer for 12 hours for homogenizing before deposition. During deposition, the particles were kept at suspension by continuous stirring of the solution by a Teflon-coated stir bar at the bottom of the beaker. In all cases during the preparation of electrodeposited coating, a Q-panel carbon steel piece (6 cm^2) and a piece of pure nickel were used as cathode and anode, respectively. The distance between the cathode and anode electrodes was kept constant at about 2 cm. The experimental setup used for preparation of coatings under different conditions can be seen in Figure 2.

2.4 Physical and chemical characterization

A scanning electron microscope or SEM was used to observe the surface and cross section morphologies of the electrodeposits. The SEM cross section allowed the determination of the coating thickness. The coating composition was analyzed by energy dispersive X-ray spectroscopy (EDS) apparatus attached to the SEM. Three randomly chosen areas were analyzed at a magnification of 500x, and an average value was calculated.

ACCEPTED MANUSCRIPT

X-ray diffraction (XRD) is a unique method for determining crystallinity. Structural analysis was performed by XRD using Cu target, Kα radiation (λ= 1.5406 Å), and operating at the scanning rate of 0.05°/s. The scanning angle range was from 20° to 95°.

From the XRD patterns, relative intensity can also be calculated to characterize the crystalline preferred orientation, using the following equations [43]:

$$R_{(hkl)} = Is_{(hkl)}/Ip_{(hkl)} \quad (1)$$

$$\text{Relative intensity} = R_{(hkl)}/\sum R_{(hkl)} \times 100\% \quad (2)$$

Where $Is_{(hkl)}$ and $Ip_{(hkl)}$ were the diffraction intensities of the (hkl) plane measured for the coatings and the standard Ni powder, respectively.

2.5 Microhardness measurement

The Vickers hardness of deposited coatings was measured by means of the Vickers microhardness technique under a load of 50gf for 15 seconds. The values stated in this study are averages of at least 5 different indentations scattered over the sample.

2.6 Wear test condition

To determine the wear resistance of the coatings, the wear tests were done using a pin-on-disc machine (POD) under unlubricated conditions. All the wear tests were performed at room temperature in the air and a chromium coated steel pin of 6mm diameter having hemispherical tip was used as the counter body. The pin and the coated sample were weighed by a balance with an accuracy of 0.1 mg before each wear test. Then they were fixed to their appropriate positions in the wear testing machine, so that the pin was vertical above the horizontal sample and touching its surface. Samples coated under different conditions were rotated for 9554 revolutions which gave a sliding distance of 180 m for the wear track diameter (6 mm) used. The sliding velocity of the machine was kept at 0.02 m/s for all the experimental runs. The stationary pin

ACCEPTED MANUSCRIPT

was pressed with the load of 200gf to the disk rotating in a horizontal plane. After wear test, the pin and coated samples were weighted to determine the wear weight loss using an electrical balance with the weight scale accuracy of 0.1 mg. Eventually, the difference between their weight before and after each test was measured. The weight loss of the coated samples was taken as a criterion for their wear behavior. The wear rate (WR) of the samples which is presented in equation (4) was acquired using the Al particle concentration measured by EDS with the assumption that the density of the coatings obeys the rule of mixtures:

$$1/(\rho_{composite}) = X_{Ni}/\rho_{Ni} + X_{Mo}/\rho_{Mo} + X_{Al}/\rho_{Al} \qquad (3)$$

Where X_{Al} is the weight fraction of Al particles in the coating and ρ_{Ni}, ρ_{Mo} and ρ_{Al} are taken as 8.9, 10.2, and 2.7 g/cm^3, respectively.

$$WR\ (m^3/N.m) = m/\rho.F.L \qquad (4)$$

Where m is the average mass loss (g), F is the applied force (N), L is the sliding distance (m), and ρ is the density of the materials (g/m^3). F and L were constant in all the tests and were not considered in the calculation. The weight change of the pin was very small in all the experiments and assuming that it was negligible, it has not been reported here.

2.7 Roughness measurement

In this study, the surface roughness parameter employed to assess surface roughness is the roughness average (Ra). Ra is internationally recognized as the commonest parameter of roughness. The roughness of the composite coatings was measured using a Mitutoyo Roughness testing instrument.

ACCEPTED MANUSCRIPT

2.8 Cathodic polarization test

All the electrochemical tests such as potentiodynamic and cathodic polarization tests were done using a potentiostat/galvanostat (EG&G model 273A) set controlled by PC. Power suite software was used to analyze this information. The working electrode was controlled by the potentiostat in a three-electrode cell equipped with a Pt counter electrode and an Ag/AgCl electrode as the reference electrode. All potentials were measured in relation to this electrode.

Potentiodynamic cathodic polarization measurements were done on the two kinds of bath solution with and without metallic ions. A Q-panel (Area = 1 cm^2) was utilized as the working electrode. Potentiodynamic cathodic polarization curves were swept from the rest potential (zero current potential) toward the more negative direction with a scan rate of 5.0 mV/sec. Figure 3 demonstrates how to acquire the partial current of hydrogen evolution ($i_{Hydrogen}$) and the total current ($i_{Hydrogen+Ni+Mo}$) using potentiodynamic cathodic polarization curves.

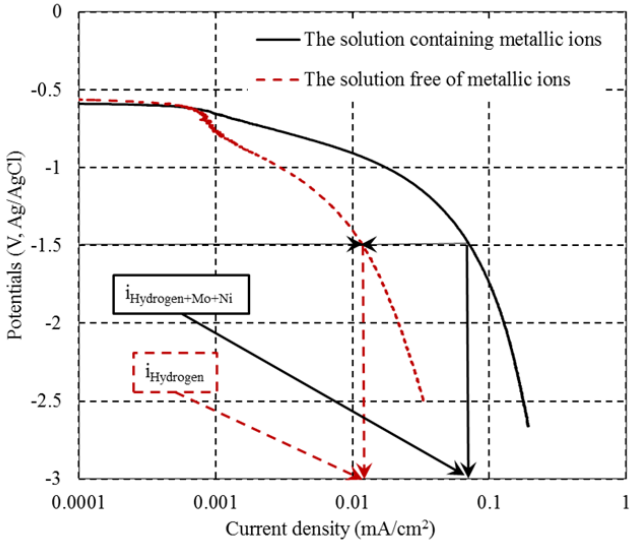

Figure 3 Schematic cathodic polarization curve for obtaining current efficiency

The current efficiency was calculated from equation (5), where η_c is the cathodic current efficiency, $i_{Hydrogen+Ni+Mo}$ is the total current density consumed by hydrogen, nickel, and

ACCEPTED MANUSCRIPT

molybdenum ions, and i_{Ni+Mo} is the partial current density only consumed by nickel and molybdenum metallic ions. A power suite software was used to analyze this information.

$$\eta_c = (i_{(Ni+Mo)}/\ i_{(Hydrogen+Ni+Mo)}) \times 100 \qquad \& \qquad i_{Ni+Mo}=i_{(Hydrogen+Ni+Mo)} - i_{(Hydrogen)} \qquad (5)$$

2.9 Potentiodynamic polarization Test

To assess the corrosion resistance of the samples, measurements were done in a 3.5wt% NaCl solution at ambient temperature in non-stirred and air free conditions using an electrochemical apparatus. Polarization curves were done at 0.5 mV/s.

The Ni-Mo/Al composite coating was the working electrode (WE). The potentiodynamic measurement was done in a range of −250 mV to +1000 mV. The surface area (0.283 cm^2) was exposed to the corrosive solution and the potentiodynamic polarization curves were recorded after 25 minutes of immersion. The corrosion potential (E_{corr}) and corrosion current density (i_{corr}) of coatings were calculated from the intersection of the cathodic and anodic Tafel curves by using the Tafel extrapolation method. The configuration of experimental setup can be observed in Figure 4.

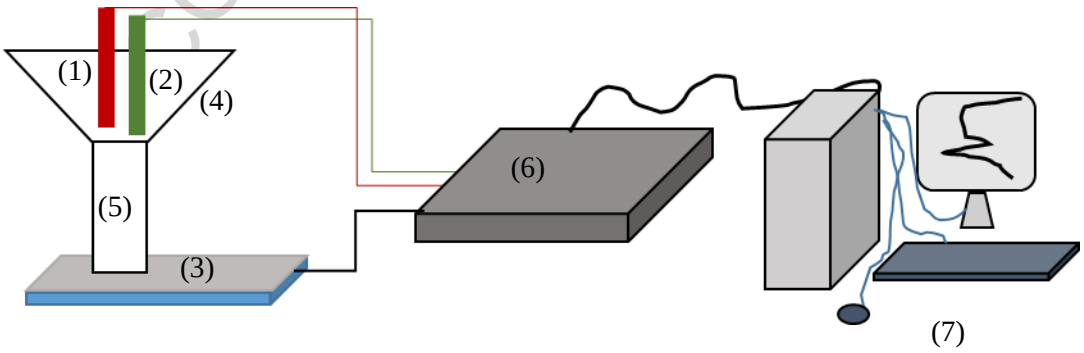

Figure 4 The configuration of experimental setup for corrosion test. (1) Counter electrode, (2) Reference electrode (3) Ni-Mo/Al composite coating as working electrode, (4) Funnel as container of corrosion solution, (5) Saline solution (3.5 wt%) as corrosion solution, (6) potentiostat/galvanostat (EG&G model 273A) set, (7) computer set (PC).

The corrosion rate was calculated according to the following equation (6) [44]:

$$(CR)= 3.27*10\text{^}(-3)\ (i_{corr} * EW/\rho) \qquad (6)$$

ACCEPTED MANUSCRIPT

Where CR, i_{corr}, EW, and ρ are the corrosion rate in mm/year, corrosion current in μA/cm^2, alloy equivalent weight in g equivalent and density in g/cm^3, respectively.

3. Results and Discussion

3.1 Determining proper bath temperature and composition

The potentiodynamic cathodic polarization curves of Ni-Mo/Al electrodeposition from the citrate baths were recorded under different bath composition and temperature conditions. Then the effect of those parameters on the cathodic current efficiency of Ni-Mo/Al composite coating bath was determined. The obtained results are shown in Figure 5. In general, the current efficiency of bath solutions containing 0.15 M citrate is much more than that of bath solutions containing 0.30 M citrate at any temperature. As seen in Figure 5, the current efficiency is not much affected by increasing temperature up to 50 ^{o}C. The highest current efficiency occurs at temperature 40^{o}C and 0.15 M citrate concentration.

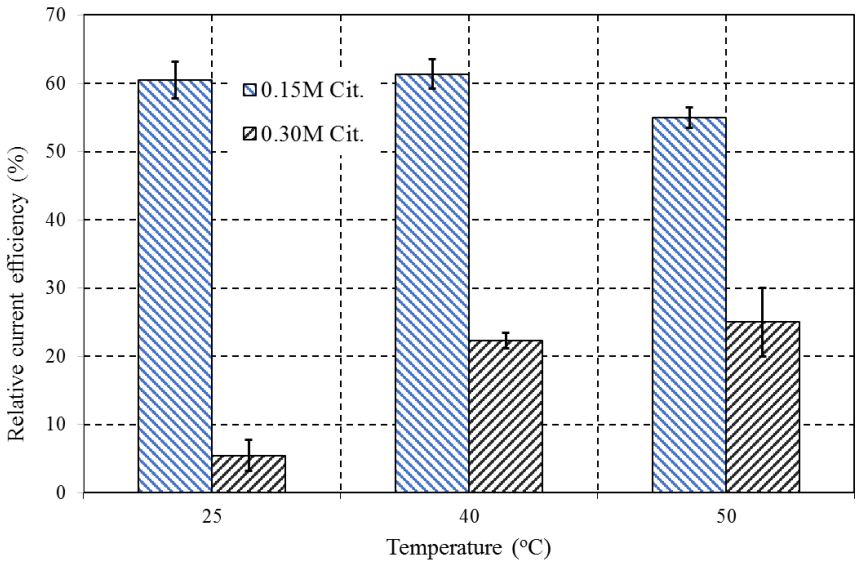

Figure 5 Current efficiency of different baths at different temperatures.

Figures 6(A) - (C) illustrate the SEM micrographs for the sample obtained at 40^{o}C and 0.15 M citrate concentration. It can be seen that Al particles were embedded in the Ni-Mo

ACCEPTED MANUSCRIPT

matrix. As is seen in Figure 7, EDS diagram demonstrates the amount of Al particles and Mo deposited in the coating. According to Figure 6, the morphology of the coating obtained at 40^{o}C is more dense and without cracks. Consequently, it seems that the nickel sulphate (0.5M) to sodium citrate (0.15M) molar ratio 3.3 is the optimum condition for obtaining nickel-based composite coatings via citrate solution bath which has also been produced and reported by Virdine and Podlaha [45].

The morphology of Ni-Mo/Al composite coatings electrodeposited under an optimum condition i.e. trial2, appears as a cauliflower structure with spherical black and white particles distributed throughout. The black and white particles were recognized by localized EDS as aluminum. The colors of aluminum particles will be discussed later.

ACCEPTED MANUSCRIPT

ACCEPTED MANUSCRIPT

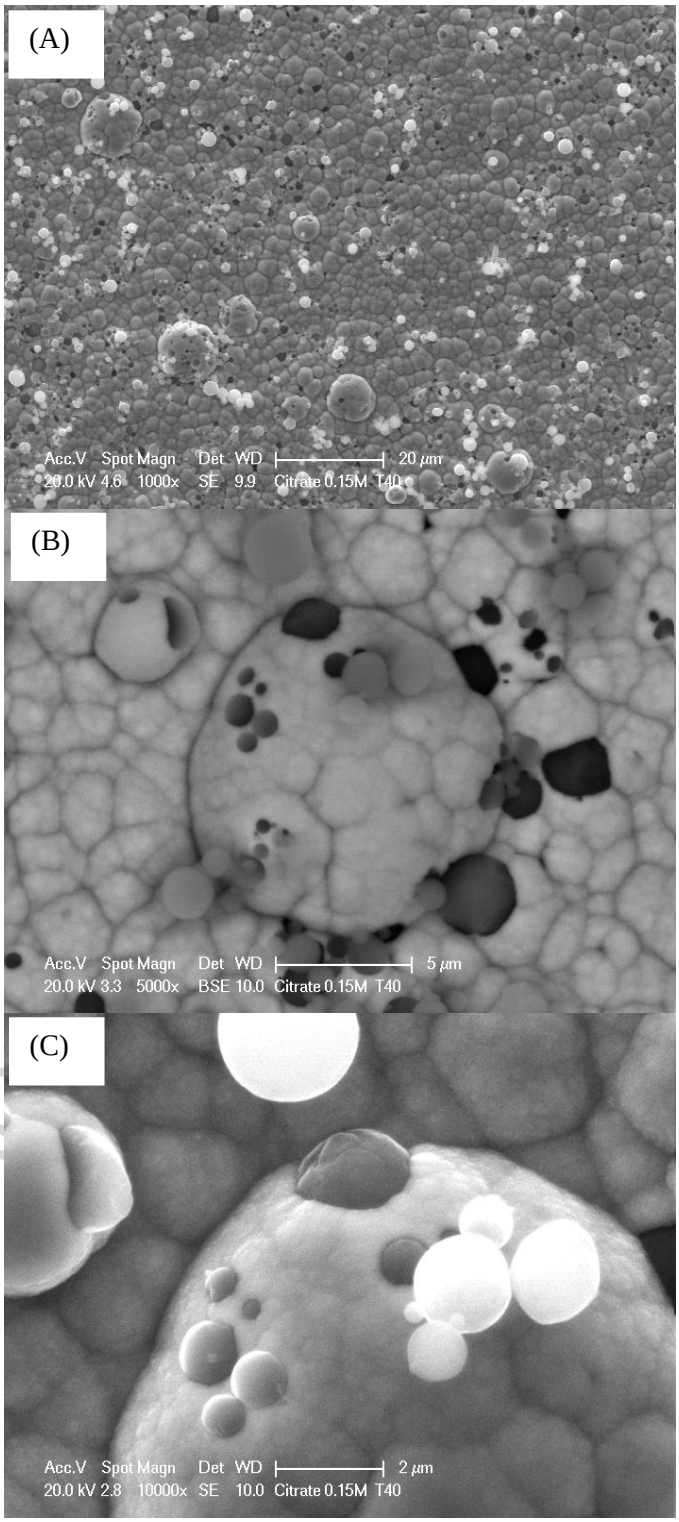

Figures 6(A)-(C) SEM micrographs for the sample obtained at citrate 0.15M and temperature 40^{o}C at different magnifications: (A) 1000x, (B) 5000x, and (C) 10000x.

The surface morphology of the Ni-Al composite coating is also given in Figure 8. Because of the presence of Mo, the morphology of the matrix changes from a regular pyramidal structure for Ni-

ACCEPTED MANUSCRIPT

Al composite coatings (Figure 8) to a cauliflower structure for Ni-Mo/Al composite coatings (Figure 6). Pitting and cracks were not observed in any of the coatings, even at a high magnification (10000x).

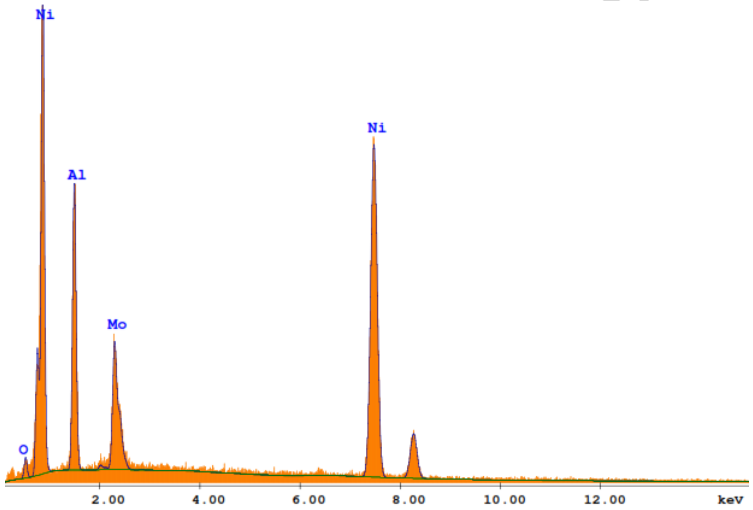

Figure 7 EDS analysis for the sample obtained at citrate 0.15M and temperature 40°C.

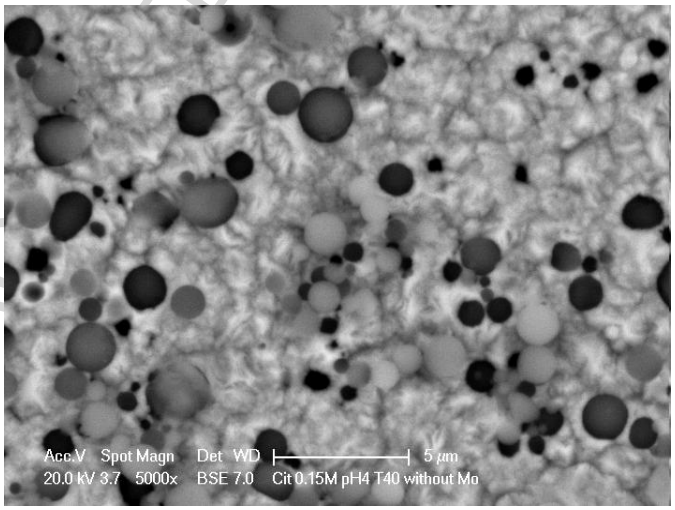

Figure 8 SEM micrograph of Ni/Al composite coating obtained identical to the conditions of trial2 (Without sodium molybdate).

The Ni-Mo/Al composite coating has a structure with finer grain sizes than the Ni-Al composite coating. An identical change in the morphology by adding Co to the Ni-Co/Al composite coating has been announced by other researchers [20]. The morphology of the matrix acquired under the

ACCEPTED MANUSCRIPT

conditions of trial2 is very identical to the matrix morphology of the Ni-Mo-Co alloy coating reported by Srivastava *et al.* [46].

As it was mentioned above, the spherical black and white particles distributed throughout the Ni/Al and Ni-Mo/Al composite coatings are Al particles. In addition to the reason suggested by Srivastava *et al.* and Bostani *et al.* [20, 27] (That some Al microparticles on the surface are covered with nickel deposit), it is demonstrated that the different colors of particles are caused by the position of particles in the coatings. Al particles were withdrawn from the surface leaving holes behind [34]. As shown in Figure 9, Al particles at different sites can be found in the coating which are incompletely surrounded by the matrix. As seen in Figure 9(B), it is clear that there is a less working distance between particle E and SEM detector compared to that of particle A. For this reason, more secondary electrons will be recognized by the detector from particle E compared to particle A. In addition to the mentioned reason, the holes on the top of particles A and B can also act as a sink and decrease the intensity of secondary electrons and deviate them. For these reasons, particle A is darker than particle B, and so on and so forth. Figure 9(C) shows the top view of different positions of Al particles embedded in the coating. It is assumed that Al particles which remain attached on the surface are strongly adsorbed on the substrate (like particle E) and will be embedded in the composite coating (like particle A).

Figure 10 demonstratesthe spectrum recorded for the Ni-Mo/Al composite coating. It illustrates that the coating was crystalline. The recorded peaks correspond to, in increasing order of 2θ, the (111), (200), (220), (311) and (222) reflections of the FCC structure of nickel. Among these, the highest reflection intensity corresponds to the (200) preferential crystallographic orientation (i.e. a highly preferred [100] growth direction) which has also been observed in references [20, 27, 47]. As can be observed, the coating is composed mainly of phases Ni, Al, and Mo metals. The

ACCEPTED MANUSCRIPT

corresponding elements are indicated on the top of each diffraction line. On the other hand, the absence of the molybdenum and aluminum oxide peaks in the XRD pattern shows that the content of these oxides in the coating surface was low with regard to the detection limit of the XRD analysis. Therefore, Ni-Mo can be considered as a solid solution with an FCC structure with Mo atoms substitutionally dissolved in Ni. Consequently, the analysis of the XRD pattern reveals the presence of a crystalline phase and reflections coming from the crystalline phase of Al microparticles. Such a phase composition confirms the composite character of the Ni-Mo/Al composite coating with the crystalline Ni-Mo alloy matrix into which Al particle is embedded.

ACCEPTED MANUSCRIPT

ACCEPTED MANUSCRIPT

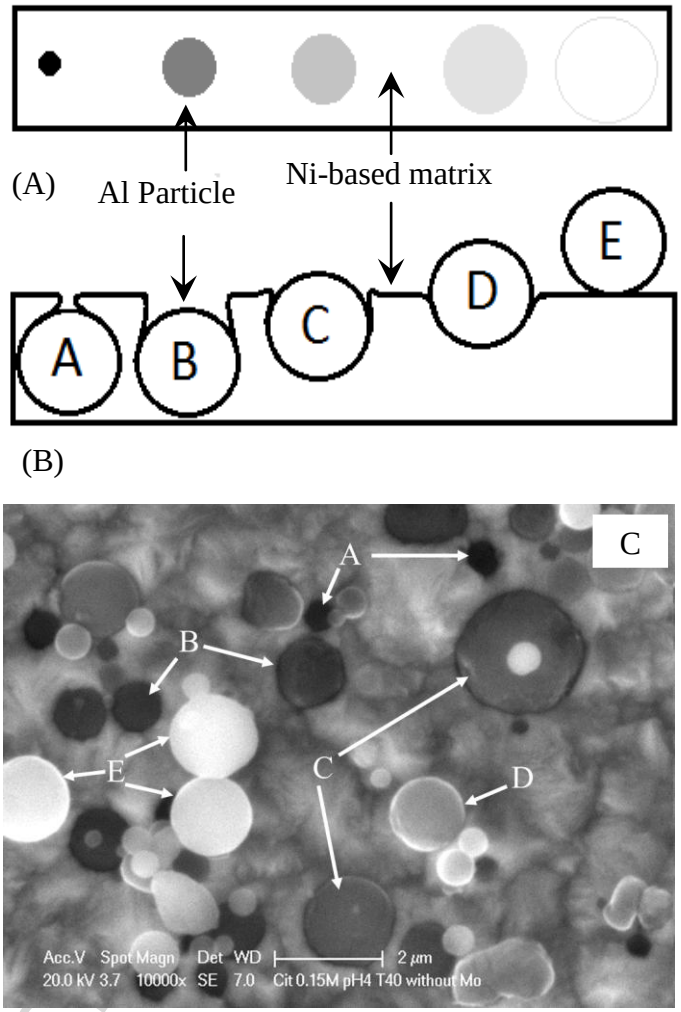

Figure 9 (A) Schematic top view of composite coating containing Al particles; (B) Schematic side view of composite coating containing Al particles; (C) Top view of Ni-Al composite coating containing Al particles as an example.

3.2The effect of Al content in the bath

As is seen in Figure 11, the Al content of the coating sharply increases to a maximum (approximately 35.6 wt%) and then weakly increases to 39 wt% by increasing the Al content in the bath.

Surface morphology of the obtained coatings at different Al contents in the bath were also studied using SEM (Figure 12). It is evident that for the co-deposited Al particles to be uniformly distributed in the Ni–Mo matrix by electrodeposition, it is important that the Al particles disperse in the electrolyte very well. Provided that the Al particles in the coatings are uniformly

ACCEPTED MANUSCRIPT

distributed, Ni–Mo/Al composite coatings could have excellent mechanical and corrosion resistance properties.

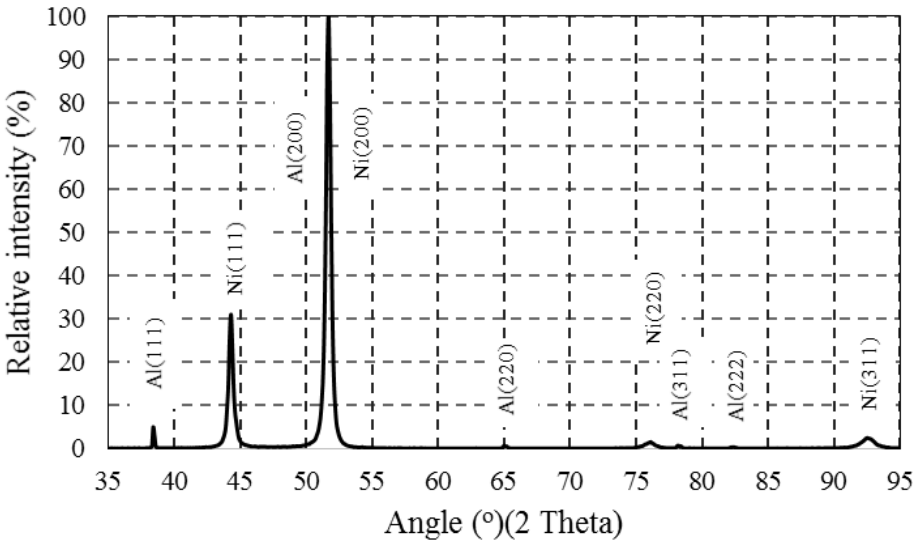

Figure 10 XRD spectra of Ni-Mo/Al composite coating obtained at trial 2.

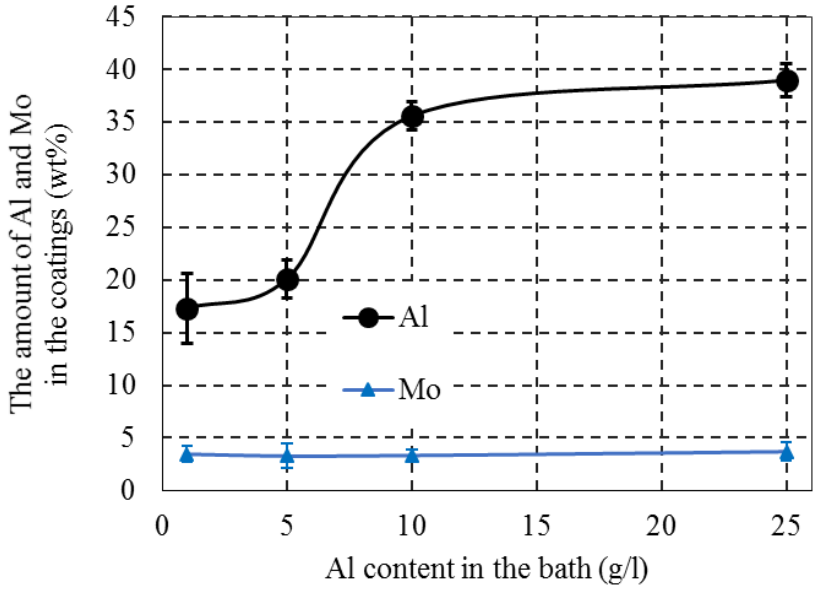

Figure 11 The Al deposited and Mo content in the coating as a function of the amount of Al particles in the bath.

The details of wear resistance estimated by WR method for different Ni-Mo/Al composite coatings obtained at different Al contents in the bath are shown in Figure 13. It is obvious that

ACCEPTED MANUSCRIPT

the WR sharply increases with increase in the Al content of the bath, reaches a maximum at 10 Al g/l and then slightly decreases by increasing Al content up to 25 g/l.

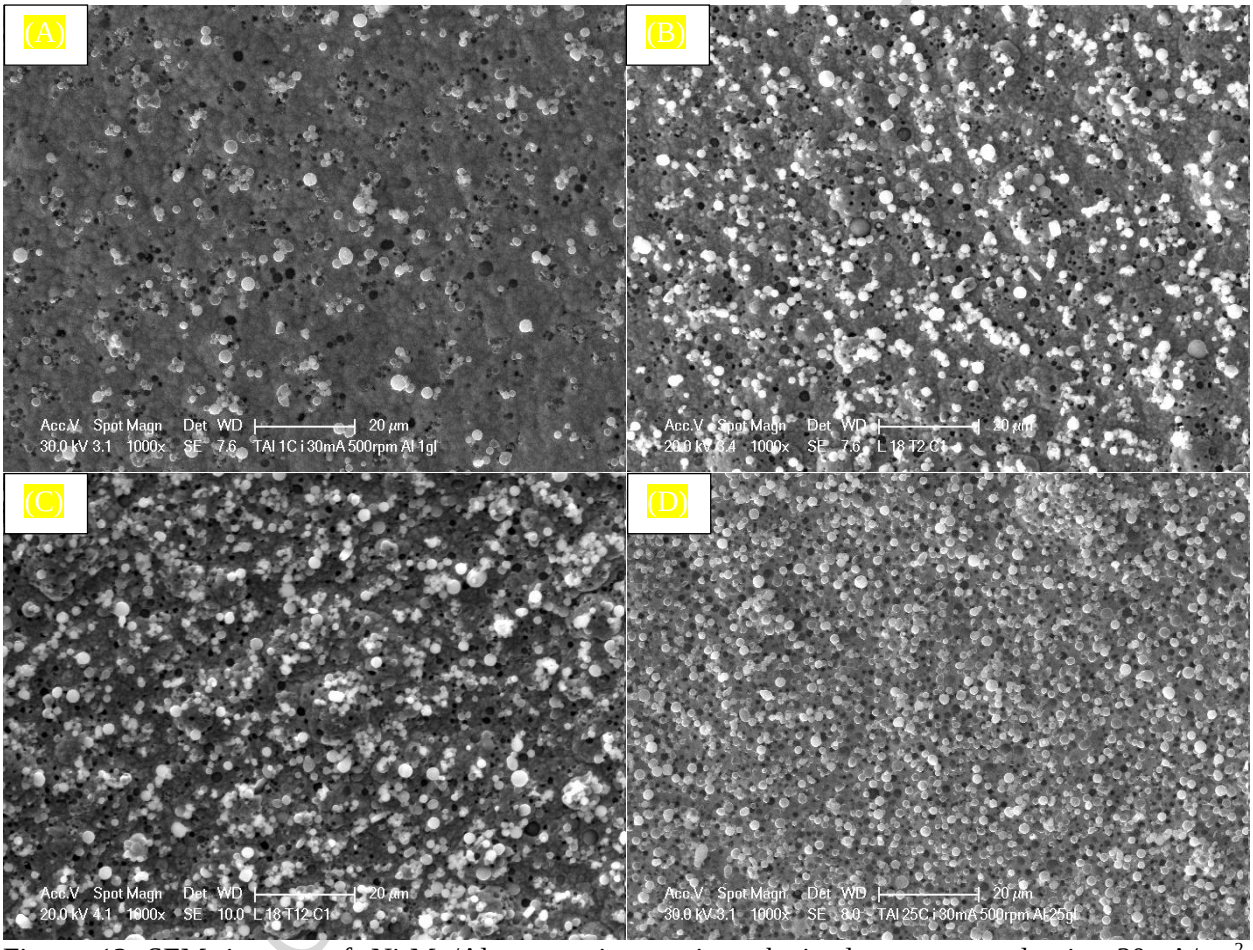

Figure 12 SEM images of Ni-Mo/Al composite coating obtained at current density 30mA/cm^2, temperature 40^{o}C, stirring rate 500rpm, and different Al contents in the solution (g/l): (A) 1, (B) 5, (C) 10, and (D) 25.

Based on the EDS results presented in Figure 11, the Al deposited in the coating was increased by increasing Al content in the bath. The WR of the coatings is also increased by increasing Al content in the coatings which indicates that increasing Al particles content in the coatings has the worst effect on their wear resistance. As it is shown in Figures 14 and 15, the roughness and microhardness of the coatings are increased and decreased, respectively. It seems that by increasing Al content in the bath, the roughness and hardness of the coatings should be increased and decreased, respectively.

ACCEPTED MANUSCRIPT

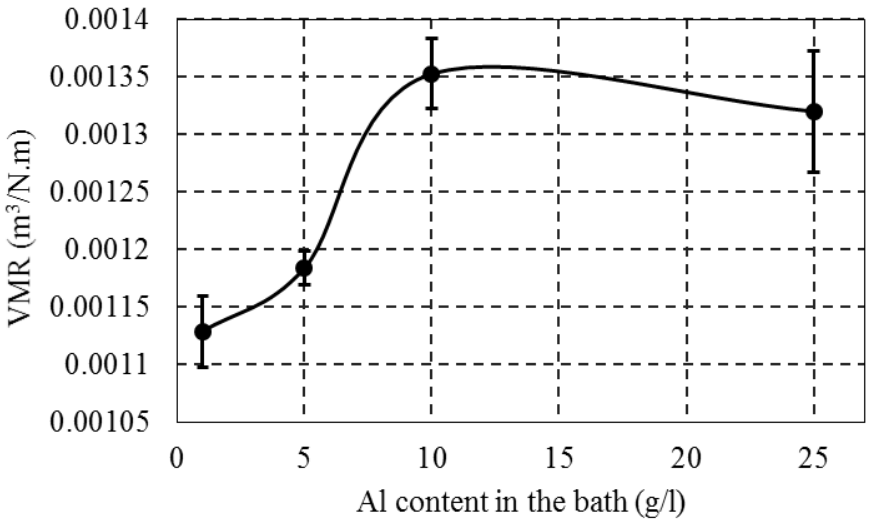

Figure 13 WR of Ni-Mo/Al composite coatings obtained in the same conditions as mentioned in the caption of Figure 12.

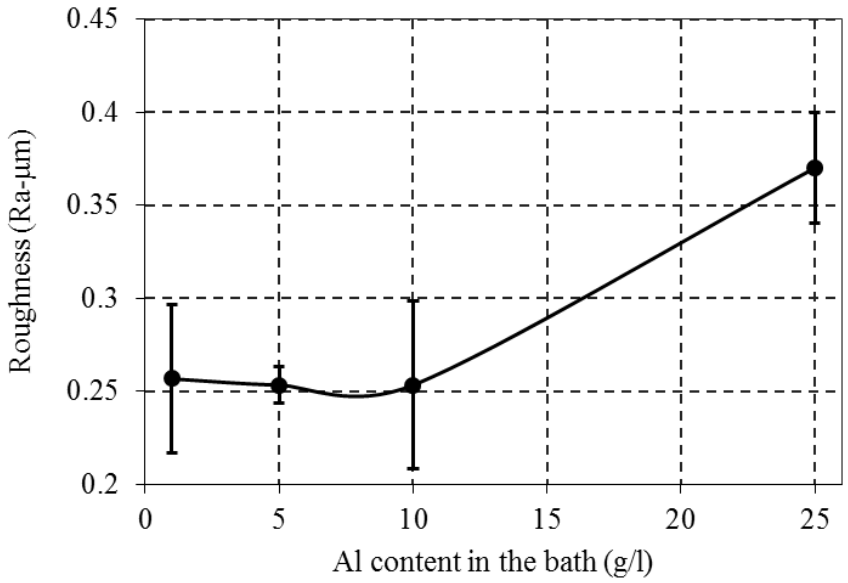

Figure 14 Surface roughness of Ni-Mo/Al composite coatings obtained at different Al contents in the bath.

According to the Archard's law [48], there is an inverse correlation between the wear behavior and surface hardness. The wear rate (WR) increases as its surface hardness decreases which validates the results of this work. On the other hand, according to the Hall-Petch relationship, although it was expected that the grain size of the coating should be increased due to decreasing hardness, Figure 16 shows peak broadening which occurred by increasing Al content in the bath.

ACCEPTED MANUSCRIPT

This can be considered as a criterion for grain refining. According to the grain refining mechanism proposed by Susan *et al.* discussed and reported in the article [26], the codeposited Al particles prevent the further growth of Ni crystallites and work as new nucleus sites, and then promote the Ni crystallites refinement.

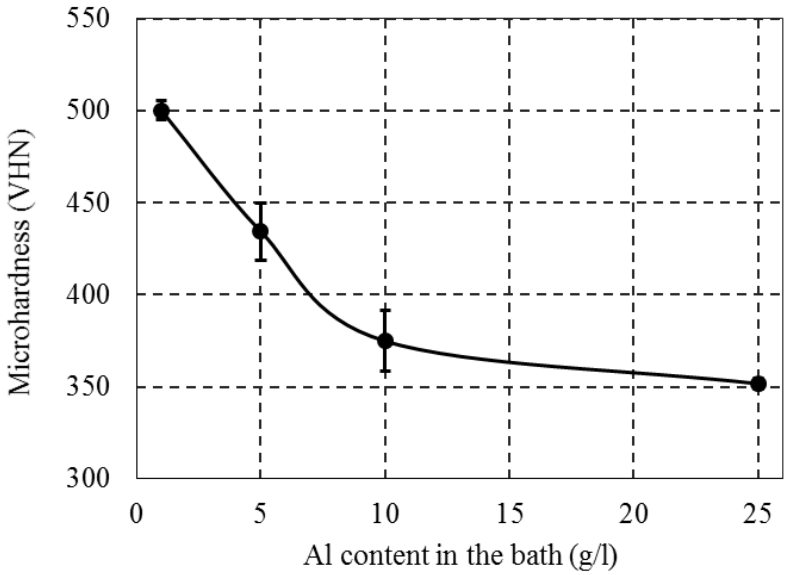

Figure 15 Microhardness of Ni-Mo/Al composite coatings obtained at different Al contents in the bath.

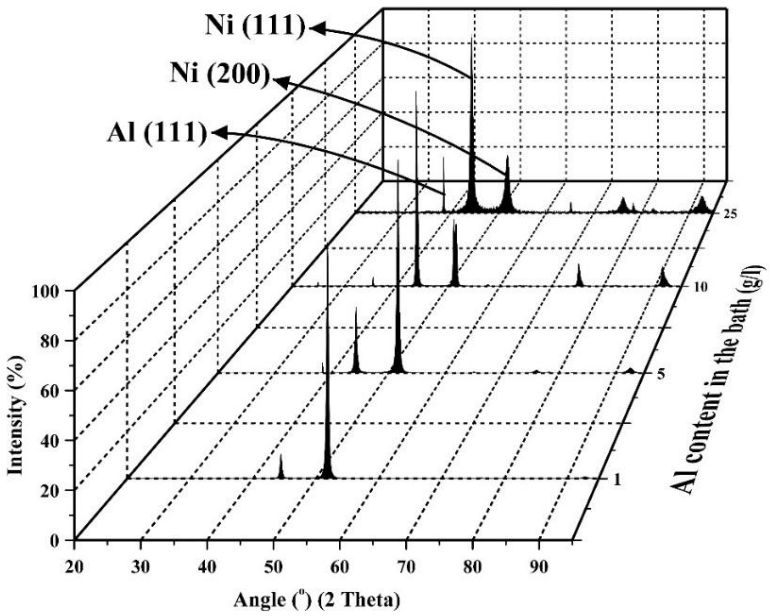

Figure 16 XRD patterns of Ni-Mo/Al composite coatings obtained at different Al contents in the bath.

ACCEPTED MANUSCRIPT

Figure 16 compares XRD patterns for the coatings electrodeposited at different Al particle loadings. It is clearly shown that when Al content in the bath is very low (1 g/l), the relative intensity of the (200) peak is very great. However, by increasing Al particle loadings in the bath, the relative intensity of the (111) peak predominated significantly. Hence, it seems that the Al particles in electrolyte contributed to the increase of [111] orientation of Ni–Mo/Al composite coating instead of [200] orientation. Consequently, it can be perceived that the microstructures of Ni–Mo coatings were influenced by the incorporation of Al particles, implying the crystal orientation evolution of the coatings [49]. Accordingly, it could be concluded that Al particles brought about electrodeposits of Ni-Mo matrix with (111) growth plane and prevented the growth of (100) plane. The level of crystal preferred orientation was assessed by plotting the relative intensity against different Al particle loadings in the bath in Figure 17. The results showed that the relative intensities (111) and (200) simultaneously increased and decreased respectively, with the increase of Al particle loadings.

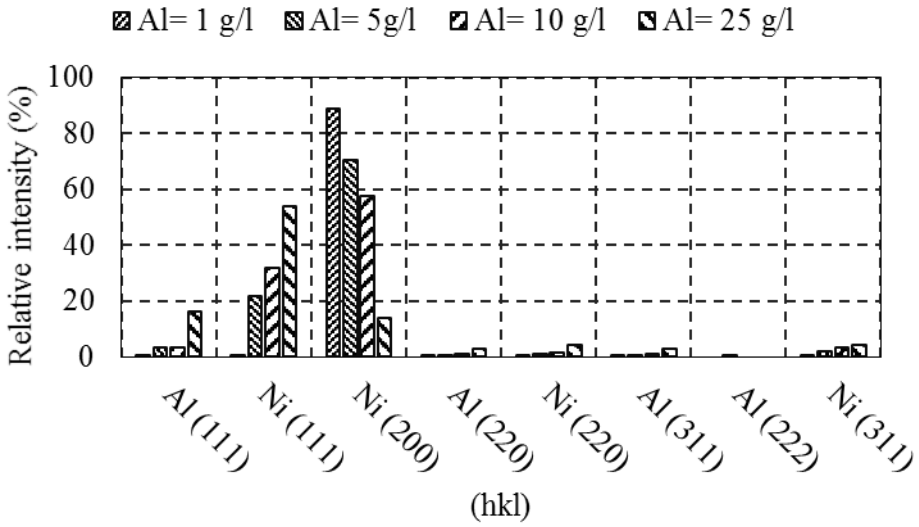

Figure 17 Relative intensity of different planes of Ni-Mo/Al composite coatings at different Al contents in the bath.

ACCEPTED MANUSCRIPT

It is clear that the presence of (111) planes with high atomic planar density and fine grains can always have a beneficial effect on the wear resistance and hardness. Thus, it was expected that the wear resistance and hardness were improved in their presence. However, as was seen in Figures 13 and 15, the wear resistance and hardness were decreased in their presence or by increasing Al contents in the bath. Accordingly, it can be concluded that the detrimental effect should be related to parameters other than the effects of crystal orientations and grain size. As a consequence, this event can be attributed to the amount of deposited Al metallic particles in the coatings and/or the metallic matrix containing hard Ni and Mo elements. Since Al metallic particles can be considered as very soft materials, decreasing the mechanical properties such as hardness can be linked to the increase of the amount of soft Al metallic particles beyond a critical value. In other words, there is a critical value of deposited Al particles in the coatings beyond which the wear resistance and hardness will be deteriorated. Decreasing the weight of hard Ni and Mo metals as the two constituents of the composite matrix can also be considered as the second detrimental factor on hardness and wear resistance. As is seen in Figure18, the maximum high deposited Ni+Mo elements is obtained at 5g/l Al loading in the bath. Then it decreases significantly by the further increase of the Al content in the bath. Finally, the wear resistance decreases with the further increase of Al content in the bath due to the weak bonding between the Ni+Mo as the composite matrix and Al deposited as reinforcement in the coating. When the amount of Al deposited in the coating is increased, the deposited Ni+Mo as the matrix cannot probably surround all the particles firmly within the matrix and the softness of the coating increases. As a result, the pin can easily damage the surface of these coatings.

The values of thickness obtained at different Al contents in the bath are also shown in Figure 19. As is seen, the thickness of coatings reaches a maximum value at 5g/l and then the change in Al

ACCEPTED MANUSCRIPT

content in the solution does not noticeably change the thickness of coatings. As a consequence, increasing Al content in the bath increases the ratio of Al particles as the reinforcement part in the composite to the amount of hard Ni+Mo metallic part as the matrix of the composite. Thus, Ni-Mo/Al composite coating will earn the properties of Al particles as the reinforcement.

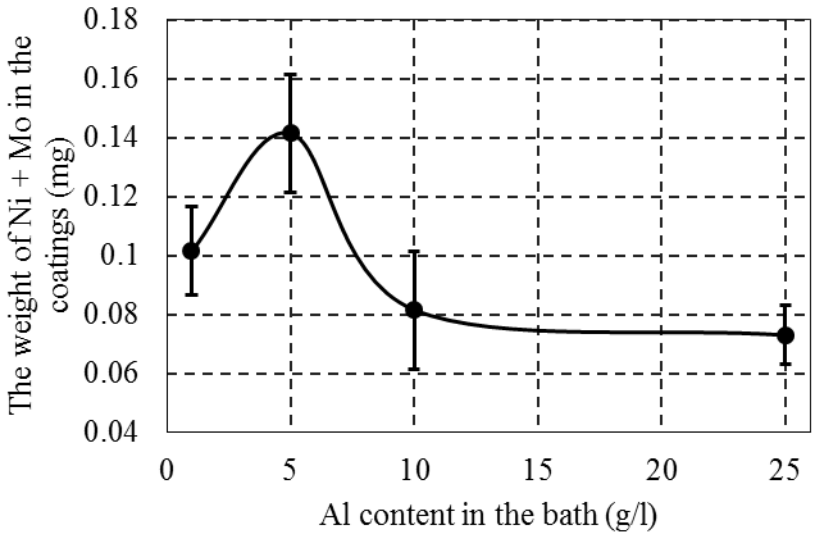

Figure 18 Weight of Ni+Mo part as the matrix of Ni-Mo/Al composite coatings obtained at different Al contents in the bath.

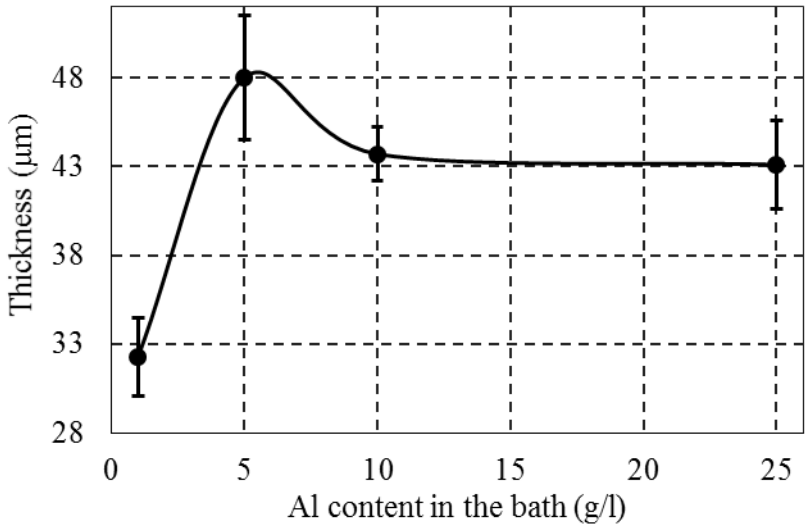

Figure 19 Thickness of Ni-Mo/Al composite coatings obtained at different Al contents in the bath.

ACCEPTED MANUSCRIPT

In addition, current efficiency can be derived from Figure 18. As can be seen, the highest efficiency is obtained at 5g/l Al content in the bath. As is observed, the efficiency is deteriorated with further increase in Al content in the bath. It means that there is an optimum value after which the Al content in the bath deteriorates the current efficiency but it does not decrease the thickness of the coating. It is reasonable that by increasing Al content in the bath, the amount of deposited Al particles which do not consume the current during electroplating, is increased. In other words,in spite of increasing the thickness of coatings by increasing Al particles, the amounts of Ni and Mo elements are decreased and consequently the main part of the current is consumed by hydrogen evolution.

Potentiodynamic polarization curves of Ni–Mo/Al composite coatings deposited at different Al contents in the bath have been presented in Figure 20. It was previously shown that the amount of Al particles in the coatings was increased by increasing Al content in the bath. In addition, the (111) planes are the predominant texture at high Al contents in the bath and the grain size is decreased by increasing Al content in the bath. As is seen in Figure 21, contrary to the negative effect of Al particles on the hardness and wear resistance mentioned above, adding Al particles to the coatings has a positive effect on their corrosion resistance. The corrosion rate of the coatings sharply decreases when the Al content increases up to 10 g/l in the bath, then it decreases only a little when the Al content in the bath goes up to 25 g/l. Thus, the improvement of corrosion resistance can be attributed to the presence of fine grain size, high Al content in the coatings, and the (111) planes, among which, it is expected that the effect of grain size on the corrosion rate is more significant than that of the others. Hence, it can be concluded that the decrease of corrosion rate with the increase of Al content in the bath is due to the decrease of the grain size.

ACCEPTED MANUSCRIPT

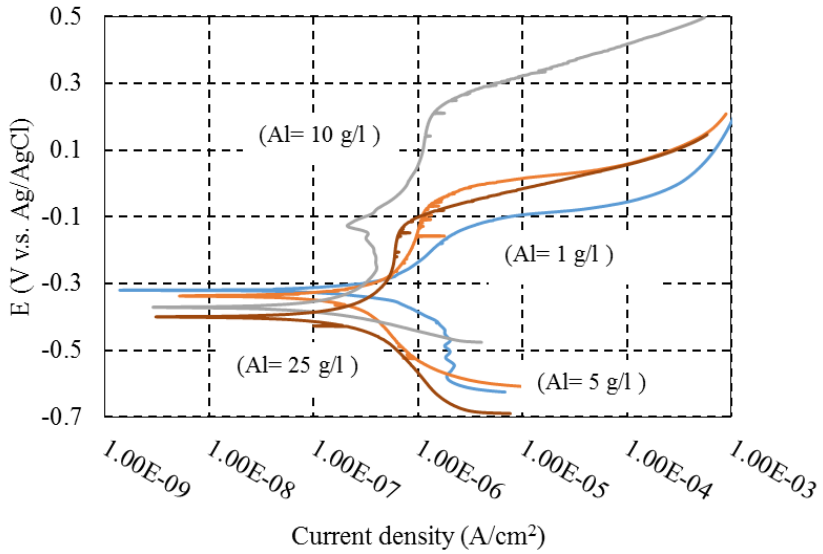

Figure 20 Potentiodynamic polarization curves of Ni-Mo/Al composite coatings at different Al contents in the bath.

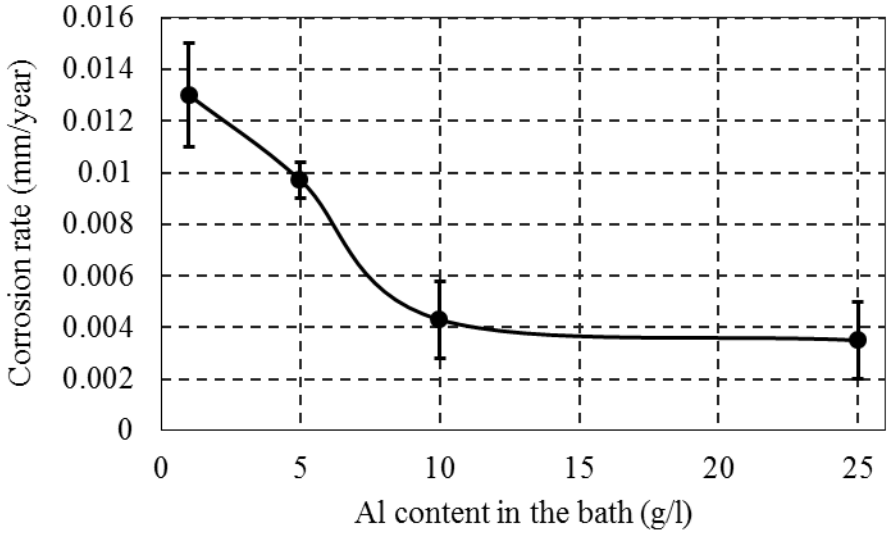

Figure 21 Corrosion rate versus Al contents in the bath.

It can be observed that there is a good agreement between the results in Figure 21 with the results reported previously [21].

3.3 Deposition mechanism of particles

Based on Guglielmi's theory [50], the Al content increases with the concentration of particles in the solution up to 25 g/l. This increase is fast from 0 to 10 g/l and slow from 10 to 25 g/l. The

ACCEPTED MANUSCRIPT

obtained curve in Figure 11 is quite similar to the well-known Langmuir adsorption isotherms, supporting a mechanism based on an adsorption effect. This relies mainly on a continuous two-step adsorption mechanism. The first step is called untight adsorption, where particles have an untight physical adsorption on the substrate with a high degree of metal ion coverage. In this step, there is a layer of adsorbed ions and solvent molecules, inhibiting the contact of the electrode and the particles. No real contact exists between cathode and particles and the adsorption is believed to be mainly physical in origin. The second step is a strong adsorption which is thought to be aided by the electric field, whereby a substantially electrochemical reaction produces a strong adsorption of powders onto the electrode. The strongly adsorbed particles are then increasingly surrounded by the growing metallic layer. Hence, in baths with low concentrations of Al (<10 g/l), the number of Ni^{2+} ion adsorbed on Al particles is small, which results in the small amount of embedded Al particles. Despite the fact that the increase of the amount of Al in the solution from 10 to 25 g/l is 2.5 times, the amount of Al deposited in the coating increases 1.1 times. In other words, at higher concentrations of Al (>10 g/ l), Ni^{2+} ions are dissolved from the anode cannot cover all Al particles, resulting in the decrease of the amount of Al particles in the coatings. Therefore, the maximum wt.% of embedded Al can be obtained from baths containing about 25 g/l of Al.

4. Conclusion

Ni-Mo/Al composite coatings were prepared via a citrate bath containing Al particles. It was demonstrated that Ni-Mo/Al composite coatings obtained at $40^{o}C$ and citrate concentration of 0.15M were dense, without crack, and had the most current efficiency. Due to the presence of Mo, the morphology of matrix is changed from a regular pyramidal structure for Ni-Al composite coatings to a cauliflower structure for Ni-Mo/Al composite coatings. The

ACCEPTED MANUSCRIPT

microhardness and wear resistance of the coatings were decreased due to the increase of Al content of the coatings. The polarization tests demonstrated that the corrosion resistance of the Ni-Mo/Al composite coating was improved by adding Al metal particles due to increase of Al content in the coatings and the decrease of the grain size of the coatings.

ACCEPTED MANUSCRIPT

ACCEPTED MANUSCRIPT

References

[1] Brooman EW. Wear behavior of environmentally acceptable alternatives to chromium coatings: nickel-based candidates. Metal Finishing. 2004;102:75-82.
[2] Srivastava M, Anandan C, Grips VKW. Ni–Mo–Co ternary alloy as a replacement for hard chrome. Applied Surface Science. 2013;285, Part B:167-74.
[3] Lima-Neto Pd, Correia AN, Vaz GL, Casciano PN. Morphological, structural, microhardness and corrosion characterisations of electrodeposited Ni-Mo and Cr coatings. Journal of the Brazilian Chemical Society. 2010;21:1968-76.
[4] Clark D, Wood D, Erb U. INDUSTRIAL APPLICATIONS OF ELECTRODEPOSITED NANOCRYSTALS NanoStruetured Materials. 1997;9:755-8.
[5] Robertson A, Erb U, Palumbo G. PRACTICAL APPLICATIONS FOR ELECTRODEPOSITED NANOCRYSTALLINE MATERIALS NanoStructured Materials. 1999;12:1035-40.
[6] Musiani M. Electrodeposition of composites: an expanding subject in electrochemical materials science. Electrochimica acta. 2000;45:3397-402.
[7] K. Helle, Walsh FC. Electrodeposition of dispersion composite coatings based upon polymer and ceramic particles in a metal matrix. Transactions of the Institute of Metal Finishing. 1997;75:53-8.
[8] C. Kerr, B.D. Barker, F.C. Walsh, Archer J. The electrodeposition of composite coatings based on metal matrix-included particle deposits, Transactions of the Institute of Metal Finishing. Transactions of the Institute of Metal Finishing. 2000;78:171-8.
[9] Walsh FC, Leon CPd. A review of the electrodeposition of metal matrix composite coatings by inclusion of particles in a metal layer: an established and diversifying technology. Transactions of the IMF. 2014;92:83-98.
[10] Roos JR, Celis JP, Fransaer J, Buelens C. The development of composite plating for advanced materials. JOM. 1990;42:60-3.
[11] Shakoor RA, Kahraman R, Waware U, Wang Y, Gao W. Properties of electrodeposited Ni–B–Al2O3 composite coatings. Materials & Design. 2014;64:127-35.
[12] Shafiee Z, Bahrololoom ME, Hashemi B. Electrodeposition of nanocrystalline Ni/Ni–Al2O3 nanocomposite modulated multilayer coatings. Materials & Design. 2016;108:19-26.
[13] Shakoor RA, Kahraman R, Waware US, Wang Y, Gao W. Synthesis and properties of electrodeposited Ni–B–CeO2 composite coatings. Materials & Design. 2014;59:421-9.
[14] Ogihara H, Wang H, Saji T. Electrodeposition of Ni–B/SiC composite films with high hardness and wear resistance. Applied Surface Science. 2014;296:108-13.
[15] Shi L, Sun C, Gao P, Zhou F, Liu W. Mechanical properties and wear and corrosion resistance of electrodeposited Ni–Co/SiC nanocomposite coating. Applied Surface Science. 2006;252:3591-9.
[16] Eslami M, Golestani-fard F, Saghafian H, Robin A. Study on tribological behavior of electrodeposited Cu–Si3N4 composite coatings. Materials & Design. 2014;58:557-69.
[17] Allahyarzadeh MH, Aliofkhazraei M, Rouhaghdam ARS, Torabinejad V. Gradient electrodeposition of Ni-Cu-W(alumina) nanocomposite coating. Materials & Design. 2016;107:74-81.
[18] Dehgahi S, Amini R, Alizadeh M. Corrosion, passivation and wear behaviors of electrodeposited Ni–Al2O3–SiC nano-composite coatings. Surface and Coatings Technology. 2016;304:502-11.
[19] Sen R, Das S, Das K. Effect of stirring rate on the microstructure and microhardness of Ni–CeO2 nanocomposite coating and investigation of the corrosion property. Surface and Coatings Technology. 2011;205:3847-55.
[20] Srivastava M, Balaraju J, Ravisankar B, Anandan C, William Grips V. High temperature oxidation and corrosion behaviour of Ni/Ni–Co–Al composite coatings. Applied Surface Science. 2012;263:597-607.
[21] Ghanbari S, Mahboubi F. Corrosion resistance of electrodeposited Ni–Al composite coatings on the aluminum substrate. Materials & Design. 2011;32:1859-64.

ACCEPTED MANUSCRIPT

[22] Susan DF, Marder AR. Oxidation of Ni–Al-Base Electrodeposited Composite Coatings. II: Oxidation Kinetics and Morphology at 1000°C. Oxidation of Metals. 2002;57:159-80.
[23] Susan DF, Marder AR. Oxidation of Ni–Al-Base Electrodeposited Composite Coatings. I: Oxidation Kinetics and Morphology at 800°C. Oxidation of Metals. 2002;57:131-57.
[24] Cai F, Jiang C, Wu X. X-ray diffraction characterization of electrodeposited Ni–Al composite coatings prepared at different current densities. Journal of Alloys and Compounds. 2014;604:292-7.
[25] Zhou Y-B, Zhang H-J. Effect of annealing treatment on cyclic-oxidation of electrodeposited Ni-Al nanocomposite. Transactions of Nonferrous Metals Society of China. 2011;21:322-9.
[26] Susan D, Barmak K, Marder A. Electrodeposited NiAl particle composite coatings. Thin Solid Films. 1997;307:133-40.
[27] Bostani B, Arghavanian R, Parvini-Ahmadi N. Study on particle distribution, microstructure and corrosion behavior of Ni-Al composite coatings. Materials and Corrosion. 2012;63:323-7.
[28] Ramesh Bapu G, Jayakrishnan S. Development and characterization of electro deposited Nickel–Titanium Carbo Nitride (TiCN) metal matrix nanocomposite deposits. Surface and Coatings Technology. 2012;206:2330-6.
[29] Narasimman P, Pushpavanam M, Periasamy VM. Synthesis, characterization and comparison of sediment electro-codeposited nickel–micro and nano SiC composites. Applied Surface Science. 2011;258:590-8.
[30] Yao Y, Yao S, Zhang L, Wang H. Electrodeposition and mechanical and corrosion resistance properties of Ni–W/SiC nanocomposite coatings. Materials Letters. 2007;61:67-70.
[31] Ogihara H, Wang H, Saji T. Electrodeposition of Ni–B/SiC composite films with high hardness and wear resistance. Applied Surface Science. 2014;296:108-13.
[32] Wang H, Yao S, Matsumura S. Electrochemical preparation and characterization of Ni/SiC gradient deposit. Journal of Materials Processing Technology. 2004;145:299-302.
[33] Tripathi MK, Singh D, Singh V. Electrodeposition of Ni-Fe/BN Nano-Composite Coatings from a Non-aqueous Bath and Their Characterization. Int J Electrochem Sci. 2013;8:3454-71.
[34] Cui X, Wei W, Liu H, Chen W. Electrochemical study of codeposition of Al particle—Nanocrystalline Ni/Cu composite coatings. Electrochimica Acta. 2008;54:415-20.
[35] Cai F, Jiang C, Fu P, Ji V. Effects of Co contents on the microstructures and properties of electrodeposited NiCo–Al composite coatings. Applied Surface Science. 2015;324:482-9.
[36] Huang P-C, Hou K-H, Sheu H-H, Ger M-D, Wang G-L. Wear properties of Ni–Mo coatings produced by pulse electroforming. Surface and Coatings Technology. 2014;258:639-45.
[37] Padilla K, Velasquez A, Berríos J, Puchi Cabrera E. Fatigue behavior of a 4140 steel coated with a NiMoAl deposit applied by HVOF thermal spray. Surface and Coatings Technology. 2002;150:151-62.
[38] Self-Bonding Composite Powders. PHELLY MATERIALS (U.S.A.) INC.
[39] Karamış M, Yıldızlı K, Çakırer H. Wear behaviour of Al–Mo–Ni composite coating at elevated temperature. Wear. 2005;258:744-51.
[40] DellaCorte C, Edmonds B. NASA PS400: a new high temperature solid lubricant coating for high temperature wear applications: National Aeronautics and Space Administration, Glenn Research Center Washington; 2009.
[41] Chen MF, Douglass DL, Gesmundo F. Sulfidation kinetics and mechanism of some Ni-Mo-Al and Ni-Al alloys over the temperature range 600–800°C. Oxidation of Metals. 1990;33.
[42] He YR, Douglass DL. The effect of Al on the corrosion behavior of Ni-Mo in a H2/H2O/H2S gas mixture. Oxidation of Metals. 1993;40:119-54.
[43] Culity B, Stock S. Elements of X-ray Diffraction. 2nd, Addition-Wesley, MA, London. 1978.
[44] Standard A. G102-89. Calculation of corrosion rates and related information from electrochemical measurements, Annual Book of ASTM Standards, ASTM International, Philadelphia. 2004.
[45] Vidrine AB, Podlaha EJ. Composite Electrodeposition of Ultrafine γ-Alumina Particles in Nickel Matrices; Part I: Citrate and chloride electrolytes. Journal of Applied Electrochemistry. 2001;31:461-8.
[46] Srivastava M, Anandan C, Grips V. Ni–Mo–Co ternary alloy as a replacement for hard chrome. Applied Surface Science. 2013;285:167-74.

ACCEPTED MANUSCRIPT

[47] Cai F, Jiang C. Influences of Al particles on the microstructure and property of electrodeposited Ni–Al composite coatings. Applied Surface Science. 2014;292:620-5.
[48] Archard J. Contact and rubbing of flat surfaces. Journal of applied physics. 1953;24:981-8.
[49] Zhao Y, Jiang C, Xu Z, Cai F, Zhang Z, Fu P. Microstructure and corrosion behavior of Ti nanoparticles reinforced Ni–Ti composite coatings by electrodeposition. Materials & Design. 2015;85:39-46.
[50] Guglielmi N. Kinetics of the deposition of inert particles from electrolytic baths. Journal of the Electrochemical Society. 1972;119:1009-12.

ACCEPTED MANUSCRIPT

ACCEPTED MANUSCRIPT

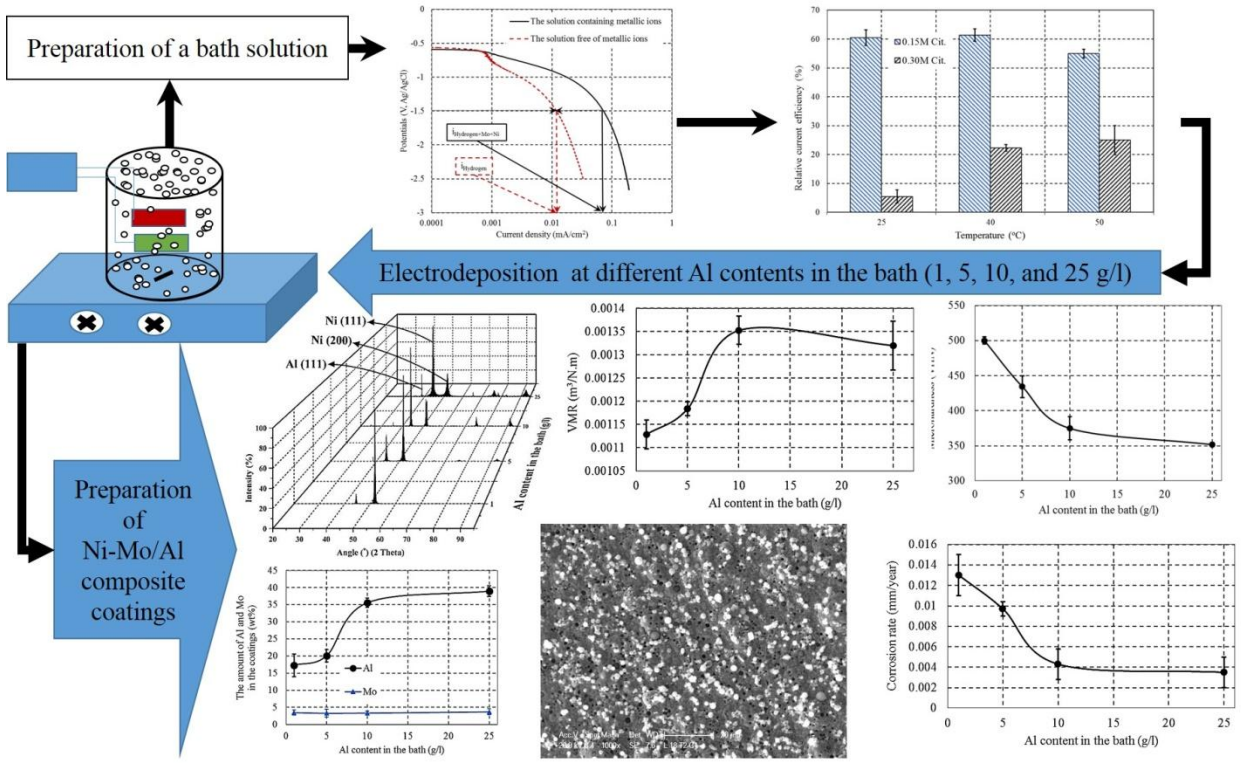

Graphical abstract

ACCEPTED

ACCEPTED MANUSCRIPT

Highlights

- Electrodeposition of Ni-Mo/Al composite coating as a new composite coating is possible.
- The Addition of Al metallic particles to the Ni-Mo alloy coatings can improve the corrosion resistance of composite coatings.
- The current efficiency is reached to a maximum and then decreased by increasing Al loading in the bath.
- It was found that there is an inverse correlation between the wear behavior and surface hardness which obeys the Archard's law.

ACCEPTED MANUSCRIPT